Metastability of Protein Solution Structures in the Absence of Solvent: Rugged Energy Landscape and Glass-Like Behavior

Tyler. C. Cropley[1,a,‡], *Fanny. C. Liu*[1‡], *Mengqi Chai*[1,b], *Matthew F. Bush*[2], *Christian Bleiholder*[1,3]*

[1] Department of Chemistry and Biochemistry, Florida State University, Tallahassee, FL 32304, USA

[2] University of Washington Department of Chemistry, Box 351700, Seattle, WA 98195-1700

[3] Institute of Molecular Biophysics, Florida State University, Tallahassee, FL 32304, USA

[a] current address: Department of Chemistry, Washington University in St. Louis, St. Louis, Missouri 63130, United States

[b] current address: Proteomics Laboratory, Division of Advanced Research Technologies, New York University Grossman School of Medicine, New York, NY 10016, United States.

‡ these authors contributed equally

*to whom correspondence should be addressed:

cbleiholder@fsu.edu
Christian Bleiholder
Florida State University
Department of Chemistry and Biochemistry
Tallahassee, FL 32304

1. *Tyler. C. Cropley, Florida State University, Tallahassee, Florida 32304, United States, Email: tyler.cropley@nyulangone.org, ORCID: 0000-0003-2804-2555.*
current address: Proteomics Laboratory, Division of Advanced Research Technologies, New York University Grossman School of Medicine, New York, NY 10016, United States

2. *Fanny Caroline Liu, Florida State University, Tallahassee, Florida 32304, United States, Email: fliu@fsu.edu, ORCID: 0000-0003-1403-7114*

3. *Mengqi Chai, Florida State University, Tallahassee, Florida 32304, United States, Email: chaim@wustl.edu, ORCID: 0000-0002-6363-0216*
current address: Department of Chemistry, Washington University in St. Louis, St. Louis, Missouri 63130, United States.

4. *Matthew F. Bush, University of Washington Department of Chemistry, Box 351700, Seattle, WA 98195-1700, United States*
Email: mattbush@uw.edu, ORCID: 0000-0003-3526-4973

5. *Christian Bleiholder, Florida State University, Tallahassee, Florida 32304, United States, Email: cbleiholder@fsu.edu, ORCID: 0000-0002-4211-1388*

ABSTRACT

Despite the significance of differentially modified proteins (proteoforms) to human health, it remains challenging to identify how proteoforms alter protein structural dynamics and function. Although native ion mobility/mass spectrometry is well-suited to handle proteoform heterogeneity, it characterizes protein structures in the absence of solvent. This raises long-standing, unanswered questions about the biological significance of structures identified through ion mobility/mass spectrometry. Using newly developed computational and experimental ion mobility/ion mobility/mass spectrometry methods, we investigate the structural denaturation of the protein ubiquitin in the solvent-free environment. We show that ubiquitin exists in the absence of solvent as an ensemble of kinetically stable subpopulations that are separated by substantial free energy barriers. These subpopulations unfold but do not interconvert, which indicates that the solvent-free subpopulations originate from different solution-phase conformations. The subpopulations exhibit stretched-exponential denaturation kinetics consistent with a glass transition associated with separating the C-terminal β-strand from the N-terminal β-hairpin occurring on the folded side of the unfolding transition state. Our data indicate that this transition state is highly polarized with significant native content in the N-terminal β-hairpin and α-helix, resembling the transition state reported for the presence of a solvent. Taken together, our analysis suggests that ubiquitin in the solvent-free environment reflects the conformational ensemble of ubiquitin in solution because the initially formed solvent-free state of ubiquitin appears glass-like and "melts" over several seconds.

Introduction

Proteins and their complexes derive their biological function from the structures they adopt and the motions through which they interconvert. While early models viewed proteins as static entities,[1] it is now widely recognized that protein function is best described in terms of an energy landscape comprising a hierarchy of conformational states and transitions between them at various scales of length, time, and energy.[2–5]

The dynamic nature of protein function takes on increased complexity in the context of cellular processes, which depend on the collective action of all proteins ("proteome"). A typical mammalian cell contains approximately one million distinct primary structures of proteins (proteoforms)[6] due to mechanisms such as post-translational modifications of proteins.[7] Altered protein primary structures can change protein interaction networks and trigger disease phenotypes,[8] as observed for RAS-related proteoforms implicated in cancer.[9–11] Therefore, elucidating how proteoforms differ in structure and dynamics is essential for understanding cellular function and dysfunction.

Mass spectrometry methods are well-suited to handle the heterogeneity arising from proteoforms or assembly steady-states and exhibit sufficient sensitivity, sample throughput, and dynamic range to enable systematic measurements of proteomes.[12–14] When combined with ion mobility spectrometry, these methods can characterize protein structures by their collision cross sections.[15] Such native ion mobility/mass spectrometry (IM/MS) methods have shown great promise in studying heterogeneous protein systems, from lipid-bound membrane proteins[16] to structurally heterogeneous glycoproteins[17] and disorder-order transitions of amyloid assemblies implicated in neurodegenerative diseases.[18–20] However, native IM/MS characterizes protein structures without solvent. Because solvent molecules stabilize proteins in their native state through the hydrophobic

effect,[21] proteins may adopt additional, non-native conformations during IM/MS analysis. For example, proteins adopt non-native, kinetically stable structures upon energetic activation,[22] and the peaks from native IM/MS measurements are typically much broader than expected for a single conformer.[23] These considerations underline that the lack of solvent raises long-standing, unaddressed questions about the extent to which IM/MS reveals biologically relevant protein structures.[24]

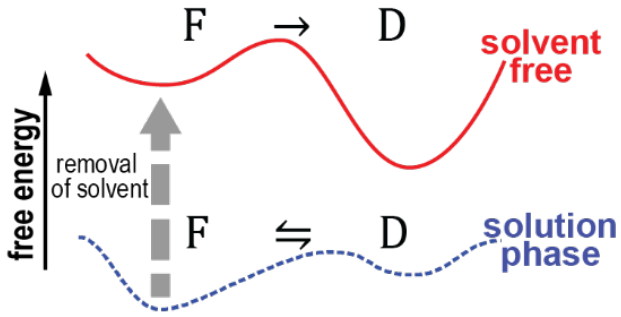

Figure 1. Energy landscapes describing protein (un)folding in the presence (blue dashed trace) and the absence (red solid trace) of solvent. In the presence of solvent, equilibrium exists between a folded (native) state ***F*** of a protein and a denatured (non-native) state ***D***. Removal of solvent shifts the barrier and free-energy profile along the unfolding coordinate and renders the folded state ***F*** less stable than the denatured state ***D***. The consequence is a structural relaxation process of a folded protein towards the (non-native) unfolded state in the solvent-free environment. Following microscopic reversibility, we discuss the relationship between the solvent-free and solvent-present protein energy landscapes.

Protein denaturation upon removal of solvent is represented by the simplified free-energy profiles in Figure 1. In the presence of solvent, equilibrium exists between a folded (native) state of a protein and an unfolded (non-native) state. Removal of solvent shifts the barrier and free-energy profile along the unfolding coordinate and renders the folded state less stable than the unfolded state. The consequence is a structural relaxation process following Arrhenius-type, single-exponential kinetics of a folded protein towards the (non-native) unfolded state in the solvent-free environment. It is empirically established that folded protein structures can be

metastable in the absence of solvent,[25–35] especially when larger protein systems are studied under gentle measurement conditions and for brief measuring times. The origin of the barriers in the solvent-free environment and strategies to increase them has garnered significant attention. For example, the complexation of charged residues on the protein surface by residual solvent[36] or crown ethers[37,38] has been proposed to prevent destabilizing interactions with the protein backbone. However, exoglycanase variants lacking charged residues exhibit gas-phase barriers comparable to wild-type that has charged surface residues and the stability of green fluorescent protein variants in the solvent-free environment appears to increase with the number of charged residues.[39] Furthermore, the contributions of entropic or enthalpic components to the energy barriers remain underexplored nor is it established how closely the metastable structures correspond to the protein native state. These gaps in understanding are significant because as a result it remains unclear how meaningful the protein structures identified by IM/MS are to study biological questions.

In the presence of solvent, several protein folding scenarios have been associated with different free energy landscapes.[40] The primary determinant for these free energy landscapes is the interplay between enthalpic stabilization by native non-covalent contacts and changes in the configurational entropy during folding.[5,41] The position of the energy barrier on the folding coordinate determines the native-ness of the transition state ensemble,[42–45] which can be polarized with native structure present only in a subset of the protein chain. Additionally, scenarios have been discussed[40,46] in which protein motions are confined to small regions in configuration space with glass-like properties of the protein.[47,48] A comparable level of understanding has not yet been accomplished for protein (un)folding in the absence of solvent. However, experimental evidence suggesting glass-like properties are available such as multi-exponential kinetics of protein unfolding and the observation of kinetic intermediates.[27–29,49]

Here, we characterize the unfolding of solvent-free ubiquitin by newly-developed computational and experimental trapped ion mobility/trapped ion mobility/mass spectrometry (tandem-TIMS/MS) methods.[34,50] These methods allow us to partition solvent-free ubiquitin into subpopulations and characterize their specific time-resolved and energy-resolved denaturation pathways. We selected bovine ubiquitin, a 76-residue globular protein, as a prototype because experimental and computational approaches have extensively characterized its solution-phase structure and dynamics.[43,51–61] The native state of ubiquitin is stable under a broad range of solution conditions[57] and shows functionally relevant structural heterogeneity at the ~50 μs time scale regime.[55] Hence, ubiquitin is simple enough that unfolding in the absence of solvent can be rigorously compared to that established in the presence of solvent. Yet, it is a sufficiently comprehensive system that the results learned may be generalizable to other protein systems. Taken together, our data indicate that ion mobility/mass spectrometry reflects the conformational ensemble of ubiquitin present in solution because the initially formed solvent-free state of ubiquitin resembles appears glass-like and "melts" over several seconds.

Experimental and Computational Details

Materials and Sample Preparation. Chicken egg white lysozyme, bovine ubiquitin, ammonium acetate, and LC/MS grade water were obtained from Sigma-Aldrich (St. Louis, MO). Ubiquitin was desalted using a 3-kDa Amicon ultra centrifugal filter (Millipore Sigma, Burlington, MA) and diluted into LC/MS grade water to a concentration of 5 μM with 1 vol% acetic acid (pH 3.5). Lysozyme was desalted and diluted into 200 mM ammonium acetate (pH 6.5) to a final concentration of 5 μM.

Tandem-TIMS/MS Measurements. A full description of the experimental settings is given in Section S1 (Supporting Information). Briefly, ion mobility measurements were performed on a

tandem-TIMS-QqTOF instrument (tandem-TIMS/MS, see Figure S1, Supporting Information) described elsewhere,[50] constructed from the coupling of two independently controlled and differentially pumped prototype TIMS[62–64] devices to a QqTOF mass spectrometer. Samples were infused into the electrospray ionization (ESI) source in positive ion mode through a gastight syringe (Hamilton, 250μL) at a flow rate of 180 μL/h. The ability of this tandem-TIMS/MS instrument for soft, native-like measurements of proteins, protein complexes, and weakly-bound peptide assemblies under these conditions has been extensively demonstrated.[34,50,65–72] Ions produced from ESI are mobility-separated in TIMS-1. Following elution from TIMS-1, ions can be mobility-selected by timing a gating voltage in the interface region as described. Mobility-selected subpopulations can be collisionally activated for collision-induced unfolding (CIU) measurements by dc-only electric fields between aperture-2 and deflector-2 (see Figure S1).[34,50,68,69,73] Time-resolved measurements can further be carried out by holding the trapping potential in TIMS-2 constant for up to ~21 seconds as described.[50,74] Subsequently, ions are mobility-separated in TIMS-2. Ion mobilities and collision cross sections were calibrated as described[75–77] using perfluorophosphazenes contained in Agilent ESI tuning mix using reported reduced ion mobilities.[76,78] The error of the calibrated cross-sections is typically less than 1 %.[76,79] Nitrogen buffer gas was used for all ion mobility measurements.

Computational details on SRA and PSA calculations. Structure relaxation approximation (SRA) calculations were carried out as described.[34] Briefly, an ensemble of all-atom protein solution structures is (de)protonated to the desired charge state(s), and short gas-phase molecular dynamics (MD) simulations are separately carried out for each protein structure using GROMACS[80] version 4.5.7 in conjunction with the OPLS/AA[81,82] force field as described.[34] The charge states observed in the experiment were attained by (de)protonating solvent accessible acidic

and basic residues as described.[34] To simulate the time-dependent unfolding of ubiquitin, we propagated each of the >1000 ubiquitin structures from the conformational ensemble for 3 μs at 450 K and stored snapshots for further analysis every 2 ns. Overall, roughly 3,000,000 collision cross-sections were computed using our projection superposition approximation (PSA)[83–86] for nitrogen gas.[87] More details are found in Section S5 (Supporting Information).

Results and Discussion

Solvent-free, compact ubiquitin subpopulations reflect the structural heterogeneity of the native state.

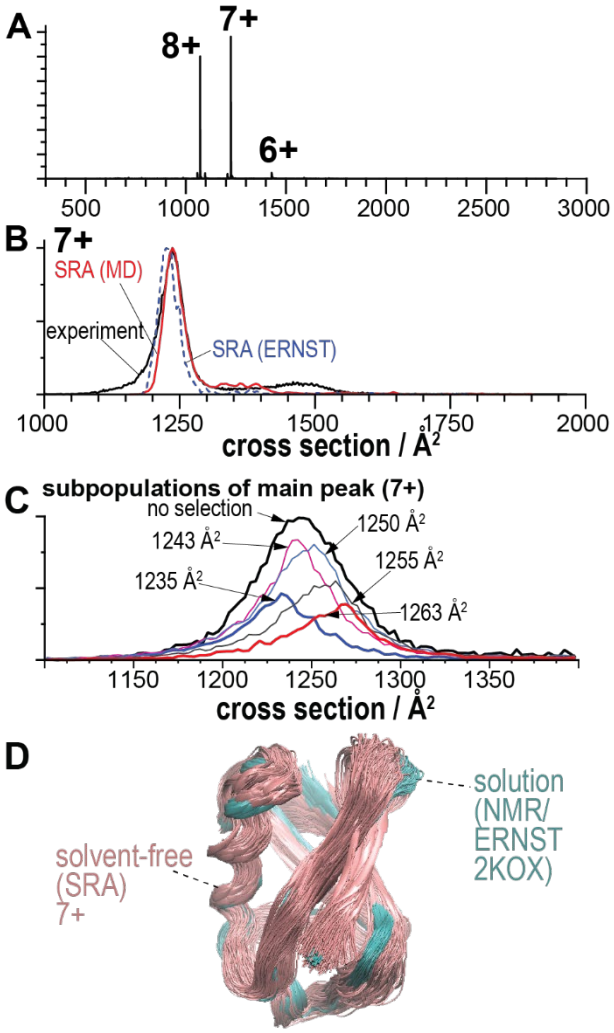

Figure 2. Solvent-free ubiquitin partitions into subpopulations that are consistent with the solution-phase conformational heterogeneity. (A) Charge states 6+ to 8+ predominate the mass spectrum of bovine ubiquitin electrosprayed from aqueous solution at pH 3.5. (B) Ion mobility spectrum for charge state 7+ showing a dominant, compact feature (black trace). Ion mobility spectra computed with our SRA method for the MD and ERNST ensembles (red traces and blue dashes, respectively) show a main, compact feature consistent with the experimental features. (C) Partitioning of the broad, compact feature (black trace) into a set of ubiquitin subpopulations (colored traces) with different collision cross sections that do not equilibrate on the ~100 ms to ~200 ms time scale of the tandem-TIMS/MS experiments. All cross sections recorded in nitrogen buffer gas. (D) Comparison between the NMR-refined ubiquitin solution ensemble and the computed ensemble for solvent-free ubiquitin (SRA).

The native state of ubiquitin is stable across various solution conditions.[57,60,61] Charge states 6+ to 8+ predominate the tandem-TIMS/MS spectra of bovine ubiquitin electrosprayed from aqueous solution at pH 3.5 (Figure 2) where its native state prevails. In line with prior literature,[34,70,87,88] the corresponding ion mobility spectra show a main compact feature with collision cross sections centered at 1186 $Å^2$ (6+), 1237 $Å^2$ (7+), and 1275 $Å^2$ (8+), respectively (see Figure 2, Figure S2 and Table S1 in the Supporting Information). The full-width-half-maxima of the dominant, compact peaks range from 44 $Å^2$ to 66 $Å^2$. This is significantly broader than expected from the instrumental resolving power and indicates unresolved conformers. Indeed, and consistent with prior literature,[26] the broad features can be partitioned into a set of subpopulations with different collision cross sections that do not equilibrate on the ~100 ms to ~200 ms time scale of the tandem-TIMS/MS experiments (Figure 2C). This means that these subpopulations differ in their structures and that structural differences are maintained for the measurement time scale.

To interpret the structure of ubiquitin in the solvent-free environment, we compared the experimental spectra to theoretical spectra computed using our structure relaxation approximation (SRA, see Figure 2 and Figure S2 in the Supporting Information).[34,69] The SRA computes ion mobility spectra from an ensemble of protein solution structures by simulating the structural

relaxation process the protein undergoes in the absence of solvent. For comparison to the experiment, we computed SRA spectra for charge states 6+ to 8+ from two reported solution-ensembles for ubiquitin: For one, a set of 1500 structures from a 600 ns explicit-solvent all-atom MD simulation used in our original description of the SRA method.[34] Second, a set of 648 ubiquitin structures refined against NMR data using the ensemble refinement for native proteins using a single alignment tensor (ERNST) approach (PDB code 2KOX).[89] Figures 2 and S2 (Supporting Information) show that the SRA spectra computed from both ensembles agree strongly with the experimental data for charge states 6+ to 8+. We emphasize that the computed ion mobility spectra reproduce the centers and relative widths of the dominant, compact peaks in the experimental spectra to within ~1 % to ~2 %, respectively (see Table S1, Supporting Information, for details), indicating a fraction of native contacts Q ~0.9 for the compact feature of charge states 6+ to 8+ with respect to the crystal structure (PDB code 1UBQ).[54] Figure 2D compares the structures computed for charge state 7+ (solvent-free, SRA) to the solution-phase ERNST ensemble,[89] underlining the structural similarity between the solvent-free subpopulations and the ubiquitin solution ensemble as probed by NMR. These results indicate that the ubiquitin subpopulations in the absence of solvent are consistent with the range of ubiquitin structures sampled in the presence of solvent.

Solvent-free ubiquitin subpopulations originate from distinct solution-phase precursors.

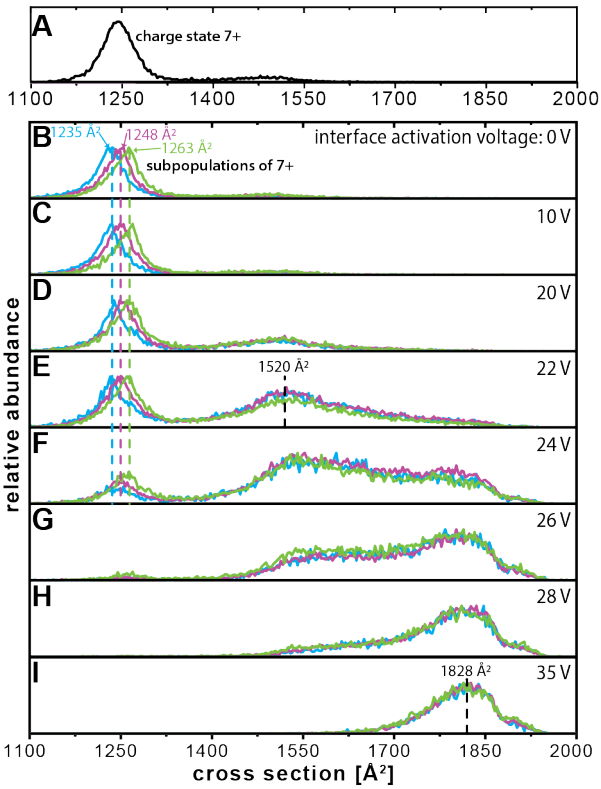

Figure 3. Interconversion of ubiquitin subpopulations requires more energy than their unfolding. (A) Compact feature of charge state 7+. (B)-(I) Traces showing mobility-selected subpopulations of the compact peak at activation voltages ranging from 0 V to 35 V. Collisional activation induces unfolding of the subpopulations but not their inter-conversion (B-E). The first intermediate species common to the unfolding of the subpopulations is a partially unfolded species centered at ~1520 Å^2 (D-F). Hence, the initially selected subpopulations do not represent distinct intermediates on a common unfolding pathway. All cross sections recorded in nitrogen gas.

If the compact, solvent-free subpopulations of ubiquitin indeed reflect the structural heterogeneity of ubiquitin in solution, then they must not stem from different degrees of unfolding of a shared solution-phase precursor structure. This proposition can be experimentally tested by probing if the subpopulations interconvert upon energetic activation: If the subpopulations originated from the same precursor structure and represent different stages of its denaturation, then they would be expected to interconvert upon activation. Hence, we selected five distinct ubiquitin subpopulations after elution from TIMS-1 (centered at 1235 Å^2, 1243 Å^2, 1248 Å^2, 1255 Å^2, and

1263 Å^2, respectively, see Table S4, Supporting Information), collisionally-activated the selected subpopulations by an applied electric field and measured the cross sections of the activated subpopulations in TIMS-2 (Figure 3).

Three observations in Figure 3 are worth commenting on. (1) The subpopulations unfold in essentially two steps *via* forming a partially unfolded feature centered at ~1520 Å^2 before an unfolded species centered at ~1830 Å^2 is formed. This observation indicates the subpopulations unfold mechanistically in a similar fashion. (2) The initially selected, compact subpopulations do not interconvert upon energetic activation. Instead, they unfold. For example, more than 50 % of the selected ions in each subpopulation have unfolded at an activation voltage of 22 V, but the initially selected compact subpopulations maintain their cross-section differences. This means that their unfolding and interconversion are distinct reactions. Further, the energy barriers for unfolding are lower than their energy barriers for interconversion. (3) The first common intermediate in the unfolding of the subpopulations is the partially unfolded species centered at ~1520 Å^2. This indicates that the structural differences between the precursors are lost once the common unfolding intermediate centered at ~1520 Å^2 has been formed. Taken together, these observations show that the selected subpopulations do not represent different degrees of denaturation of a shared precursor species in the solvent-free environment. Hence, the most likely scenario is that the subpopulations observed in the absence of solvent originate from structurally distinct solution-phase precursors.

Stretched-exponential unfolding kinetics suggest a glass-like state of folded, solvent-free ubiquitin.

Our discussion above shows that the subpopulations are separated by energy barriers sufficiently high so that their interconversion requires more energy than their unfolding. This indicates that the free energy barriers confine the molecular motions of the subpopulations into disjoint regions in

configuration space. This notion is reminiscent of amorphous solids or glassy materials,[90,91] where energy barriers locally confine motions in configuration space and render transitions between components too slow to occur on the observation time scale.

Because structural relaxation processes of glassy systems exhibit stretched-exponential time-dependent characteristics,[3,90,91] the above considerations prompted us to investigate the kinetics of the structural relaxation process of the ubiquitin (sub)populations in the solvent-free environment. To this end, we mobility-selected ubiquitin ions eluting from TIMS-1 and stored the selected ions in TIMS-2 for up to ~21 seconds before recording ion mobility spectra. Figure 4 shows time-resolved ion mobility spectra recorded by trapping compact ubiquitin for charge states 6+ and 7+ for up to ~21 seconds in TIMS-2. The corresponding time-resolved spectra for the compact populations of charge state 8+ for ubiquitin are given in Figure S5 (Supporting Information). As controls, we recorded time-resolved spectra for lysozyme (charge state 8+), the partially unfolded feature of charge state 7+ of ubiquitin (aqueous solution, after collisional activation) and the partially unfolded feature of charge state 8+ of ubiquitin from acidic methanol:water (see Figures S5 to S7, Supporting Information, for details).

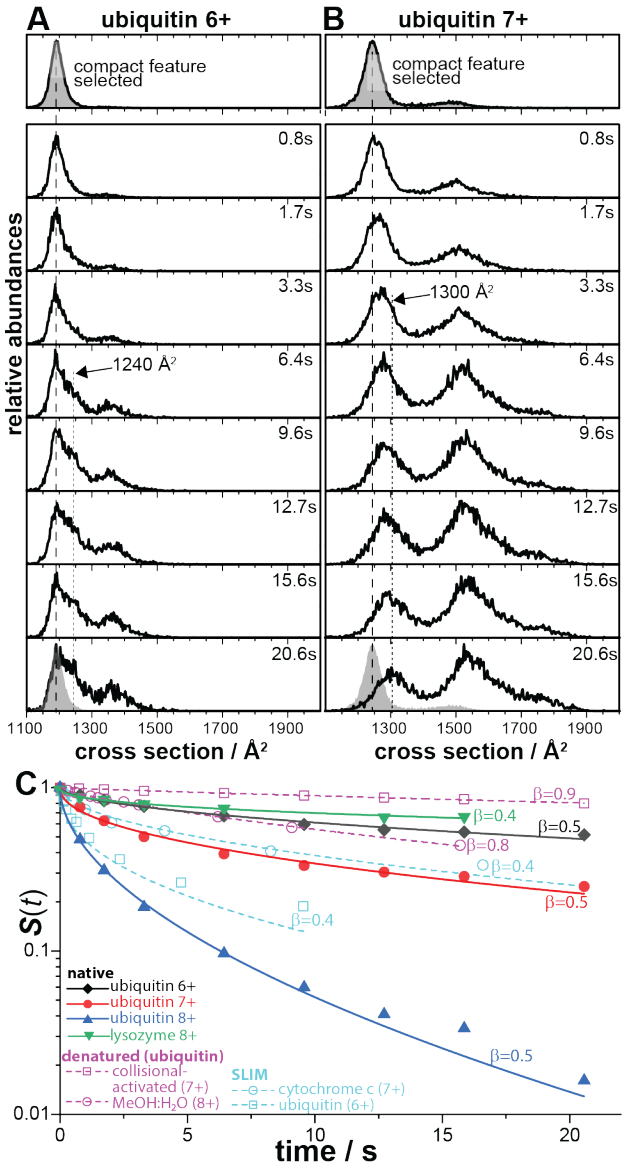

Figure 4. Unfolding of compact protein species follows stretched-exponential kinetics with a stretching coefficient β of ~0.5 consistent with glasses. (A, B) Time-resolved ion mobility spectra for ubiquitin charge states 6+ and 7+ (black traces). The compact feature (gray trace) was selected and stored in the absence of solvent for up to ~21 s, showing the formation of a transiently populated intermediate at cross sections of ~1250 Å^2 (6+) and ~1300 Å^2 (7+), respectively, before a partially unfolded species at ~1400 Å^2 (6+) and ~1550 Å^2 (7+), respectively, emerges. (C) Survival yields $S(t)$ for native-like ubiquitin (6+, 7+, 8+) and lysozyme 8+ (filled symbols), non-native (partially unfolded) ubiquitin (7+, 8+, pink, open symbols) obtained from the overlap between the compact feature of the mobility-selected spectrum and the spectrum after storage. SLIM-measurements (cyan, open symbols) taken from

references [49] (ubiquitin 6+) and [29] (cytochrome c 7+). Note the logarithmic y-sale. The curves show fitted stretched exponentials $S(t) = e^{-(kt)^{\beta}}$ underlining stretched-exponential relaxation for the folded, compact species ($\beta \approx 0.4$ - 0.5) but Arrhenius-type single-exponential kinetics for the denatured (partially unfolded) species ($\beta \approx 0.8$ and 0.9). All cross sections recorded in nitrogen buffer gas.

The time-resolved spectra (Figures 4 and S5, Supporting Information) show the structural relaxation of compact ubiquitin (charge states 6+ to 8+) into a stable, unfolded species (1800 Å^2 - 2000 Å^2) *via* a partially unfolded intermediate (1400 Å^2 - 1700 Å^2). The unfolded and partially unfolded species are consistent with those observed by CIU (Figure 3). However, a difference to the CIU spectra is the emergence of an elongated yet compact transient intermediate (~1250 Å^2 for charge state 6+ and ~1300 Å^2 for 7+ and 8+) discussed in detail in the next section.

We first tested if the structural relaxation of the compact ubiquitin ions exhibits exponential time-dependent characteristics. Figure 4C shows the survival yields $S(t)$ for the compact features of ubiquitin charge states 6+ to 8+ upon storage for up to ~21 s in TIMS-2. As negative controls, we plot $S(t)$ for partially unfolded ubiquitin conformations produced from acidic aqueous methanol and upon collisional activation of the compact species, respectively. As positive controls, we show $S(t)$ for lysozyme (charge state 8+) and prior data for cytochrome c and ubiquitin recorded on SLIM-type instruments.[29,49] A two-state reaction results in single-exponential kinetics according to $S(t) = \exp(-kt)$. Such exponential kinetics are observed for the structural relaxation of the denatured (partially unfolded) ubiquitin species (see Figure 4 and Figure S6, Supporting Information), but excluded for all compact protein species from non-denaturing conditions (see Figure S8, Supporting Information). We further discarded all kinetic models that posit an equilibrium between the compact and the partially unfolded species, because structural relaxation of the partially unfolded species did not produce detectable amounts of compact ubiquitin conformations within the ~21 s measurement time scale (see Figure S6, Supporting Information).

In line with literature reports,[27–29] $S(t)$ can be fit to a double-exponential rate law at high confidence, but this leads to overfitting even for its 3-parameter form (see Figure S9, Supporting Information). By contrast, high goodness of fit was achieved without overfitting for the simpler stretched-exponential rate law $S(t) = \exp\left[-(kt)^{\beta}\right]$ with only the rate constant k and the stretching coefficient β as fitting parameters. The resulting rate constants k increase roughly 25-fold from charge states 6+ to 8+ of ubiquitin (see Table S5, Supporting Information), as expected from literature reports.[25,27,49] What is more intriguing is that the corresponding stretching coefficients β for the compact, native-like protein systems cluster around $\beta \approx 0.4$ to 0.5, indicative of a strongly stretched-exponential relaxation process. By contrast, the stretching coefficients for the denatured controls are $\beta \approx 0.8$ and $\beta \approx 0.9$, respectively, more in line with Arrhenius-type kinetics. Thus, time-resolved measurements for three proteins on two distinct types of ion mobility/mass spectrometers suggest that the structural relaxation of compact, native-like proteins is strongly stretched-exponential.

A structural relaxation process with stretched-exponential kinetics can have two different origins.[92] For a scenario of glass-like protein ions, the structural relaxation process occurs on a rough free energy landscape with kinetic traps due to "molecular frustration" and each ion structurally relaxes in a stretched-exponential manner. The alternative scenario is that of an ensemble of unresolved protein ions that each react exponentially but with a broad distribution of rate constants. Hence, we further probed the origin of the observed stretched-exponential relaxation kinetics by characterizing the relaxation process of mobility-selected ubiquitin subpopulations with cross sections ranging from 1235 Å^2 to 1263 Å^2 (see Figure 5 and the Supporting Information for Table S4 and Figures S11, S12).

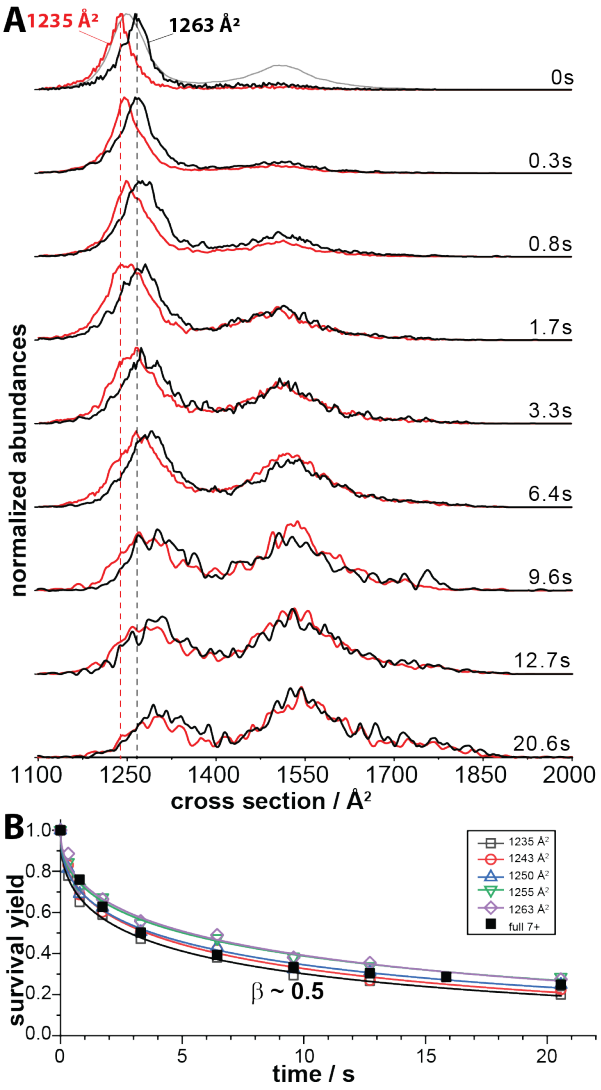

Figure 5. Ubiquitin subpopulations follow stretched-exponential kinetics with a stretching coefficient β~0.5. (A) Time-resolved ion mobility spectra for ubiquitin charge state 7+ subpopulations centered at 1235 Å^2 (red trace) and 1263 Å^2 (black trace). The selected distributions maintain their cross-section differences for up to ~2 s. All subpopulations transiently populate a compact species with a cross-section of ~1300 Å^2 before forming the partially unfolded species, and relative abundances of the partially unfolded species are comparable. (B) Survival yields $S(t)$ of the compact features for the selected subpopulations as a function of the storage time. The data show that all subpopulations unfold in stretched-exponential kinetics with β~0.5. All cross sections recorded in nitrogen buffer gas.

We make three observations from the time-resolved spectra of the mobility-selected subpopulations plotted in Figure 5. First, all selected subpopulations transiently populate an intermediate with a cross-section of ~1300 $Å^2$ before forming the partially unfolded species centered at ~1525 $Å^2$. Further, the positions and relative abundances of the transient intermediate at ~1300 $Å^2$ and partially unfolded species centered at ~1525 $Å^2$ appear comparable for all subpopulations at all trapping times. These observations indicate that the unfolding pathway and kinetics are similar for the subpopulations. Second, structural differences of the selected subpopulations are maintained for approximately 2 s, and interconversion of the subpopulations before their respective unfolding is not observed. Finally, fitting the survival yields $S(t)$ to stretched exponentials results in stretching coefficients $\beta \approx 0.5$ consistent with the value obtained for the entire compact population of charge state 7+ (Figure 5B). Hence, our data are most consistent with the view that unfolding occurs on a rough free energy landscape that results in stretched-exponential unfolding kinetics.

We observed stretched-exponential structural relaxation for three protein systems recorded on two distinct ion mobility/mass spectrometry platforms. By contrast, we found Arrhenius-type, exponential relaxation kinetics for structural relaxation of denatured species. The fitted stretching coefficients β cluster around 0.4 to 0.5 for stretched-exponential kinetics for three protein systems and several charge states recorded on two instrument types. These values for the stretching coefficients β are similar to the expected value of β =3/7 for glasses influenced by Coulombic interactions.[90] Hence, the fitted values for β of roughly 0.4 to 0.5 seem reasonable for the structural relaxation of charged protein systems in a glass-like state. Because the stretched exponential function is economical with only two fitting parameters, it seems unlikely that the success of fitting all data shown here in a consistent manner is entirely by accident. Hence, our data strongly support

a scenario of a glass transition occurring between the initially present compact ubiquitin states and the partially denatured state.

Ubiquitin unfolds through a polarized transition state, regardless of solvents.

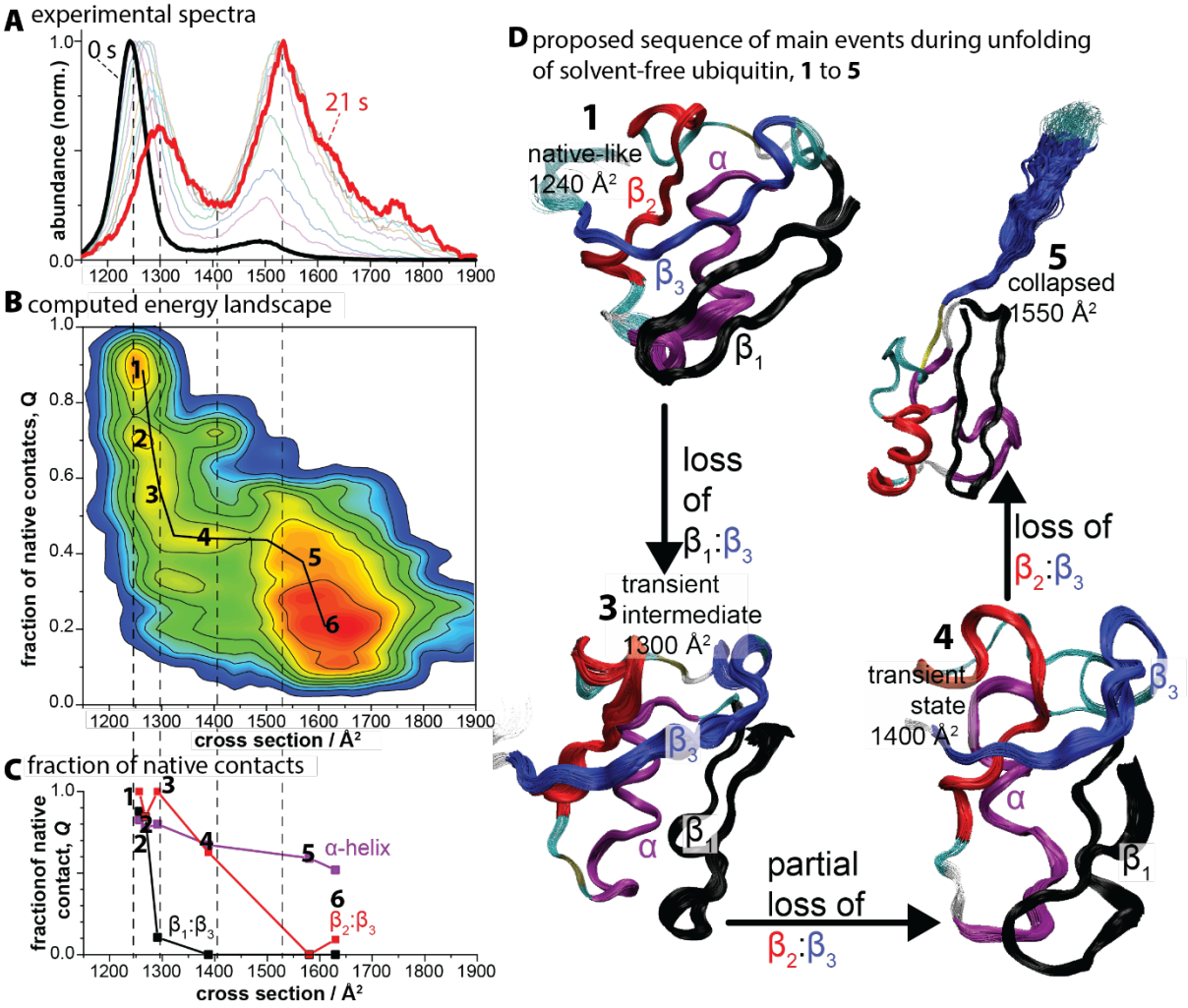

Figure 6. Solvent-free ubiquitin unfolds on a rugged energy landscape *via* a highly polarized transition state with native character on the N-terminus. (A) Time-dependent ion mobility spectra for storage of charge state 7+ up to ~21 s (from Figure 4B, superimposed). The experimental ion abundances partition into two regions of significant intensity that are separated by a minimum of ion abundances around 1400 Å^2. (B) Energy landscape $W(\Omega, Q) = -\ln w(\Omega, Q)$ compiled from MD simulations where $w(\Omega, Q)$ is the number of structures encountered at cross-section Ω and fraction of native contacts Q. The computed landscape mirrors the experimental data showing two broad basins associated with compact (Ω < 1400 Å^2) and partially unfolded (Ω > 1500 Å^2) conformations. These two basins are connected by

a "bottleneck" in the computed landscape at cross sections of roughly 1460 Å^2, closely matching the free energy maximum inferred from the experimental spectra at cross section of ~1400 Å^2. (C) The fraction of native contacts for different secondary structure elements of ubiquitin for the minima found in the energy landscape $W(\Omega, Q)$, showing that the C-terminus separates (**1**, **2**, **3**) from the N-terminus on the folded side of the transition state (**4**). The α-helix retains native content and proximity to the N-terminal β-region on the denatured side of the transition state (**5**, **6**). (D) The proposed sequence of events of ubiquitin unfolding in the solvent-free environment based on the energy landscape shown in (B). All cross sections recorded in nitrogen buffer gas.

To interpret the structural changes occurring in the time-resolved unfolding measurements, we probed the structural relaxation process of compact ubiquitin charge state 7+ using MD simulations (Figure 6). To this end, we propagated each of the >1000 structures computed by the SRA for the compact feature of charge state 7+ (Figure 2D) for 3 μs using solvent-free MD simulations and calculated cross sections using our PSA method for structures sampled every 2 ns. We then used the "reactive" trajectories that reached the partially unfolded species with cross sections >1500 Å^2 to approximate an energy landscape describing the structural relaxation process (Figure 6B). We represented the sampled structures by their fraction of native contacts, Q, and collision cross-section Ω. The fraction of native contacts, Q, correlates roughly with the enthalpic stabilization of the polypeptide chain by native non-covalent interactions, whereas the collision cross section enables direct comparison to the experimental spectra and is a measure for the compactness, and therefore the configurational entropy, of the polypeptide chain.

We observe a strong consistency between the experimental time-resolved spectra (Figure 6A) and the energy landscape compiled from the unfolding simulations (Figure 6B). First, the ion abundances in the measured spectra can be broadly partitioned into two regions of significant intensity that are separated by a minimum of ion abundances around 1400 Å^2. Hence, ubiquitin structures with cross sections around 1400 Å^2 appear less stable than those smaller or larger than

~1400 Å^2. The experimental spectra thus indicate a maximum in the free energy for ubiquitin conformations with cross sections around 1400 Å^2, which separates "compact" conformations (Ω < 1400 Å^2) from "partially unfolded" conformations (Ω > 1400 Å^2). The computed energy landscape mirrors these experimental observations, showing two broad basins associated with compact (Ω < 1400 Å^2) and partially unfolded (Ω > 1500 Å^2) conformations. Further, these two basins are connected by a "bottleneck" in the computed energy landscape at cross sections of roughly 1460 Å^2, closely matching the free energy maximum inferred from the experimental spectra at cross sections of ~1400 Å^2. Second, the abundance maximum in the compact basin shifts from ~1250 Å^2 to ~1300 Å^2 over several seconds in the experimental spectra. This means ubiquitin unfolds in the solvent-free environment via a transient population of intermediate conformations with a roughly 3 % to 5 % larger cross section before reaching the free energy maximum at ~1400 Å^2. This observation is reproduced by the computed energy landscape showing a local minimum at ~1300 Å^2 on-pathway to the partially unfolded basin.

The observed agreement between the experimental and computed data allows us to identify the motions describing the structural transitions in the experimental spectra from the simulations. Taken together, our data suggest the following pathway for unfolding of ubiquitin in the absence of solvent (Figures 6C, 6D): First, the C-terminal β-strand separates from the N-terminal β-hairpin while the N-terminal β-hairpin and α-helix remain strongly native. This leads to the intermediate species with a cross-section of ~1300 Å^2, maintaining an overall compact structure ($\Delta\Omega \leq 5\%$) at a significant loss of native contacts ($\Delta Q \approx 0.5$). Hence, the formation of this compact, transient intermediate at ~1300 Å^2 is dominated by the loss of energetically stabilizing native contacts without a substantial increase in configurational entropy. Next, the C-terminal β_3-strand separates from the β_2-strand whereas the N-terminal β-hairpin and α-helix remain strongly native. This leads

through the transition region with a "bottleneck" in the energy landscape at ~1460 Å^2 and connects to the basin of partially unfolded conformations with cross sections of ~1550 Å^2. This process is associated with a substantial increase in configurational entropy ($\Delta\Omega \approx 20\%$) at the modest loss of native contacts ($\Delta Q < 0.2$). Subsequently, native contacts are lost in the N-terminal β-hairpin while maintaining an overall collapsed state with the α-helix maintaining some native-like contacts. Finally, this collapsed state can unfold to conformations with strongly elongated ubiquitin polypeptide chains (see Figure S6, Supporting Information, note that this occurs on a time scale beyond the 21 s available for our measurements for charge states 6+ and 7+).

Following microscopic reversibility, our data indicate that ubiquitin unfolding in the solvent-free environment shares many characteristics with that established for the presence of solvent:[51–53,58,59] (1) Regardless of the presence of solvent, unfolding of ubiquitin starts by separation of the C-terminal β-strand from the scaffold of ubiquitin and this step occurs on the folded side of the transition state. (2) The transition state appears polarized with a predominant native structure in the N-terminal region of the β-hairpin and the α-helix. In contrast, the remainder of the polypeptide chain does not exhibit a strongly native character. (3) At the denatured side of the transition state, a collapsed state maintains a nucleus by closely packing the N-terminal β-hairpin and α-helix, both with some extent of native character.

Summary and Conclusions

We characterized the unfolding of ubiquitin in the absence of solvent by a combination of newly developed computational and experimental ion mobility/ion mobility/mass spectrometry methods. To this end, we partitioned solvent-free, folded ubiquitin ions into subpopulations that do not interconvert on the measurement time-scale. We then experimentally probed their collision-induced unfolding (CIU) and time-resolved structural relaxation processes. We computed ion

mobility spectra for comparison to the experiment and to interpret the structural changes during the unfolding processes observed in the experiment. Our data show:

(1) The computed ion mobility spectra indicate that the ubiquitin subpopulations reflect the structural heterogeneity of ubiquitin in the solution phase (Figure 1).

(2) The subpopulations unfold upon energetic activation but do not interconvert. This means that they are confined into disjoint regions in configuration space by substantial free energy barriers, and that the free energy barriers for interconversion are larger than those for unfolding. Hence, the subpopulations most likely originate from different solution-phase precursors (Figures 2 and 3).

(3) The unfolding pathway of ubiquitin in the solvent-free environment share characteristics with that established for the presence of solvent (Figure 6). Our experimental and computed data suggests that unfolding begins by separation of the C-terminal β-strand at a significant loss of enthalpic stabilization without increase of configurational entropy. This process produces a slightly elongated intermediate at substantial loss of native contacts, all on the folded side of the transition state. The transition state appears polarized with significant native content in the N-terminal β-hairpin and α-helix as reported for the solution phase. This transition state leads to a collapsed state with a partially native α-helix in proximity to the N-terminal β-hairpin. This process is associated with a significant increase in configurational entropy without substantial change in native contacts.

(4) The time-dependent structural relaxation of the subpopulations exhibits strongly stretched-exponential kinetics with stretching coefficients β clustering around ~0.4 to ~0.5 (Figures 4 and 5). By contrast, Arrhenius-type, exponential kinetics are observed on the unfolded side of the transition state. The data suggest a glass transition on the folded side of the transition

state due to rugged free energy landscape associated with loss of contacts between the C-terminal β-strand and the N-terminal β-hairpin.

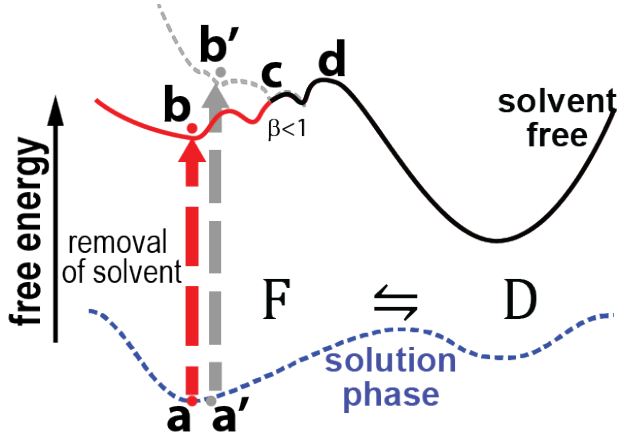

Figure 7. Energy landscapes summarizing our interpretation of the computational and experimental data on the unfolding of solvent-free ubiquitin discussed in the current work. Different solution conformers (**a**, **a'**) populate different solvent-free subpopulations upon removal of solvent (**b**, **b', Figures 2 and 3**). The different subpopulations undergo stretched-exponential structural relaxation on a rugged energy surface and lose their structural differences (**c, Figures 4 and 5**). The transition state region for ubiquitin appears highly polarized with native content at the N-terminus as proposed for the transition state in the presence of solvent (**d**, **Figure 6**). Our data are consistent with a glass transition between (**b**), (**b'**) and (**d**).

Figure 7 summarizes our interpretation of our data. Different ubiquitin solution-phase conformers are transferred into the solvent-free environment as non-interconverting subpopulations separated by significant free energy barriers. The structural relaxation of the subpopulations follows stretched-exponential kinetics due to rugged free energy surface. The data are consistent with the assumption of a glass-like transition on the folded side of the transition state similar to Type II energy landscapes.[40] These considerations suggest that the persistence of native protein structures in the absence of solvent may result from a glass-like state of the initially formed solvent-free protein. In this state, the disruption of native non-covalent interactions leads to

"frustration" and a rugged energy landscape, manifested as stretched-exponential structural relaxation kinetics.

ASSOCIATED CONTENT

Supporting Information. Expanded experimental and computational details with seven tables and 11 Figures related to native time-resolved and energy-resolved IM/MS analysis of proteins.

AUTHOR INFORMATION

Corresponding Author

*cbleiholder@fsu.edu

Author Contributions

Conceptualization & Methodology: CB and FCL; Investigation and formal analysis: TC, FCL, MC, CB. Original draft: CB, TC. Review and Editing: all authors. All authors have approved the final version of the manuscript. ǂThese authors contributed equally.

ACKNOWLEDGMENT

The authors thank Dr. Thais Pedrete for assistance in carrying out some of the time-dependent measurements. This work was supported by the National Institutes of Health under grant R01GM135682 (CB) and by the National Science Foundation under Grants No. CHE-1654608 (CB) and CHE-2305173 and (CB). Research reported in this publication was supported by the National Institute of General Medical Sciences of the National Institutes of Health through award number R01GM130708 (MFB).

REFERENCES

(1) Perutz, M. F.; Brunori, M. Stereochemistry of Cooperative Effects in Fish and Amphibian Haemoglobins. *Nature* **1982**, *299* (5882), 421–426.
(2) Onuchic, J. N.; Wolynes, P. G. Theory of Protein Folding. *Curr. Opin. Struct. Biol.* **2004**, *14* (1), 70–75.
(3) Frauenfelder, H.; Sligar, S. G.; Wolynes, P. G. The Energy Landscapes and Motions of Proteins. *Science* **1991**, *254* (5038), 1598–1603.
(4) Li, Z.; Raychaudhuri, S.; Wand, A. J. Insights into the Local Residual Entropy of Proteins Provided by NMR Relaxation. *Protein Sci.* **1996**, *5* (12), 2647–2650.
(5) Dobson, C. M.; Šali, A.; Karplus, M. Protein Folding: A Perspective from Theory and Experiment. *Angew. Chem. Int. Ed.* **1998**, *37* (7), 868–893.
(6) Aebersold, R.; Agar, J. N.; Amster, I. J.; Baker, M. S.; Bertozzi, C. R.; Boja, E. S.; Costello, C. E.; Cravatt, B. F.; Fenselau, C.; Garcia, B. A.; Ge, Y.; Gunawardena, J.; Hendrickson, R. C.; Hergenrother, P. J.; Huber, C. G.; Ivanov, A. R.; Jensen, O. N.; Jewett, M. C.; Kelleher, N. L.; Kiessling, L. L.; Krogan, N. J.; Larsen, M. R.; Loo, J. A.; Ogorzalek Loo, R. R.; Lundberg, E.; MacCoss, M. J.; Mallick, P.; Mootha, V. K.; Mrksich, M.; Muir, T. W.; Patrie, S. M.; Pesavento, J. J.; Pitteri, S. J.; Rodriguez, H.; Saghatelian, A.; Sandoval, W.; Schlüter, H.; Sechi, S.; Slavoff, S. A.; Smith, L. M.; Snyder, M. P.; Thomas, P. M.; Uhlén, M.; Van Eyk, J. E.; Vidal, M.; Walt, D. R.; White, F. M.; Williams, E. R.; Wohlschlager, T.; Wysocki, V. H.; Yates, N. A.; Young, N. L.; Zhang, B. How Many Human Proteoforms Are There? *Nat. Chem. Biol.* **2018**, *14* (3), 206–214.
(7) Yang, X.; Coulombe-Huntington, J.; Kang, S.; Sheynkman, G. M.; Hao, T.; Richardson, A.; Sun, S.; Yang, F.; Shen, Y. A.; Murray, R. R.; Spirohn, K.; Begg, B. E.; Duran-Frigola, M.; MacWilliams, A.; Pevzner, S. J.; Zhong, Q.; Trigg, S. A.; Tam, S.; Ghamsari, L.; Sahni, N.; Yi, S.; Rodriguez, M. D.; Balcha, D.; Tan, G.; Costanzo, M.; Andrews, B.; Boone, C.; Zhou, X. J.; Salehi-Ashtiani, K.; Charloteaux, B.; Chen, A. A.; Calderwood, M. A.; Aloy, P.; Roth, F. P.; Hill, D. E.; Iakoucheva, L. M.; Xia, Y.; Vidal, M. Widespread Expansion of Protein Interaction Capabilities by Alternative Splicing. *Cell* **2016**, *164* (4), 805–817.
(8) Li, Y. I.; van de Geijn, B.; Raj, A.; Knowles, D. A.; Petti, A. A.; Golan, D.; Gilad, Y.; Pritchard, J. K. RNA Splicing Is a Primary Link between Genetic Variation and Disease. *Science* **2016**, *352* (6285), 600–604.
(9) Iversen, L.; Tu, H.-L.; Lin, W.-C.; Christensen, S. M.; Abel, S. M.; Iwig, J.; Wu, H.-J.; Gureasko, J.; Rhodes, C.; Petit, R. S.; Hansen, S. D.; Thill, P.; Yu, C.-H.; Stamou, D.; Chakraborty, A. K.; Kuriyan, J.; Groves, J. T. Ras Activation by SOS: Allosteric Regulation by Altered Fluctuation Dynamics. *Science* **2014**, *345* (6192), 50–54.
(10) Tsai, F. D.; Lopes, M. S.; Zhou, M.; Court, H.; Ponce, O.; Fiordalisi, J. J.; Gierut, J. J.; Cox, A. D.; Haigis, K. M.; Philips, M. R. K-Ras4A Splice Variant Is Widely Expressed in Cancer and Uses a Hybrid Membrane-Targeting Motif. *Proc. Natl. Acad. Sci.* **2015**, *112* (3), 779–784.
(11) Harper, K. L.; Sosa, M. S.; Entenberg, D.; Hosseini, H.; Cheung, J. F.; Nobre, R.; Avivar-Valderas, A.; Nagi, C.; Girnius, N.; Davis, R. J.; Farias, E. F.; Condeelis, J.; Klein, C. A.; Aguirre-Ghiso, J. A. Mechanism of Early Dissemination and Metastasis in Her2+ Mammary Cancer. *Nature* **2016**, *540* (7634), 588–592.
(12) Meier, F.; Brunner, A.-D.; Frank, M.; Ha, A.; Bludau, I.; Voytik, E.; Kaspar-Schoenefeld, S.; Lubeck, M.; Raether, O.; Bache, N.; Aebersold, R.; Collins, B. C.; Röst, H. L.; Mann, M. diaPASEF: Parallel Accumulation–Serial Fragmentation Combined with Data-Independent Acquisition. *Nat. Methods* **2020**, *17* (12), 1229–1236.

(13) Benesch, J. L. P.; Ruotolo, B. T.; Simmons, D. A.; Robinson, C. V. Protein Complexes in the Gas Phase: Technology for Structural Genomics and Proteomics. *Chem. Rev.* **2007**, *107* (8), 3544–3567.
(14) Kondrat, F. D. L.; Struwe, W. B.; Benesch, J. L. P. Native Mass Spectrometry: Towards High-Throughput Structural Proteomics. In *Structural Proteomics*; Owens, R. J., Ed.; Methods in Molecular Biology; Springer New York: New York, NY, 2015; Vol. 1261, pp 349–371.
(15) Lanucara, F.; Holman, S. W.; Gray, C. J.; Eyers, C. E. The Power of Ion Mobility-Mass Spectrometry for Structural Characterization and the Study of Conformational Dynamics. *Nat. Chem.* **2014**, *6* (4), 281–294.
(16) Laganowsky, A.; Reading, E.; Allison, T. M.; Ulmschneider, M. B.; Degiacomi, M. T.; Baldwin, A. J.; Robinson, C. V. Membrane Proteins Bind Lipids Selectively to Modulate Their Structure and Function. *Nature* **2014**, *510* (7503), 172–175.
(17) Roberts, D. S.; Mann, M.; Melby, J. A.; Larson, E. J.; Zhu, Y.; Brasier, A. R.; Jin, S.; Ge, Y. Structural O-Glycoform Heterogeneity of the SARS-CoV-2 Spike Protein Receptor-Binding Domain Revealed by Top-Down Mass Spectrometry. *J. Am. Chem. Soc.* **2021**, *143* (31), 12014–12024.
(18) Bleiholder, C.; Bowers, M. T. The Solution Assembly of Biological Molecules Using Ion Mobility Methods: From Amino Acids to Amyloid β-Protein. *Annu. Rev. Anal. Chem.* **2017**, *10* (1), 365–386.
(19) Bernstein, S. L.; Dupuis, N. F.; Lazo, N. D.; Wyttenbach, T.; Condron, M. M.; Bitan, G.; Teplow, D. B.; Shea, J.-E.; Ruotolo, B. T.; Robinson, C. V.; Bowers, M. T. Amyloid-β Protein Oligomerization and the Importance of Tetramers and Dodecamers in the Aetiology of Alzheimer's Disease. *Nat. Chem.* **2009**, *1* (4), 326–331.
(20) Bleiholder, C.; Dupuis, N. F.; Wyttenbach, T.; Bowers, M. T. Ion Mobility–Mass Spectrometry Reveals a Conformational Conversion from Random Assembly to β-Sheet in Amyloid Fibril Formation. *Nat. Chem.* **2011**, *3* (2), 172–177.
(21) Callaway, D. J. E. Solvent-Induced Organization: A Physical Model of Folding Myoglobin. *Proteins Struct. Funct. Genet.* **1994**, *20* (2), 124–138.
(22) Brandon T. Ruotolo; Suk-Joon Hyung; Paula M. Robinson; Kevin Giles; Robert H. Bateman; Carol V. Robinson. Ion Mobility–Mass Spectrometry Reveals Long-Lived, Unfolded Intermediates in the Dissociation of Protein Complexes. *Angew. Chem. Int. Ed.* **2007**, *46*, 8001–8004.
(23) Allen, S. J.; Giles, K.; Gilbert, T.; Bush, M. F. Ion Mobility Mass Spectrometry of Peptide, Protein, and Protein Complex Ions Using a Radio-Frequency Confining Drift Cell. *The Analyst* **2016**, *141* (3), 884–891.
(24) Breuker, K.; McLafferty, F. W. Stepwise Evolution of Protein Native Structure with Electrospray into the Gas Phase, 10-12 to 102 s. *Proc. Natl. Acad. Sci.* **2008**, *105* (47), 18145–18152.
(25) Wyttenbach, T.; Bowers, M. T. Structural Stability from Solution to the Gas Phase: Native Solution Structure of Ubiquitin Survives Analysis in a Solvent-Free Ion Mobility–Mass Spectrometry Environment. *J. Phys. Chem. B* **2011**, *115* (42), 12266–12275.
(26) Koeniger, S. L.; Merenbloom, S. I.; Clemmer, D. E. Evidence for Many Resolvable Structures within Conformation Types of Electrosprayed Ubiquitin Ions. *J. Phys. Chem. B* **2006**, *110* (13), 7017–7021.

(27) Myung, S.; Badman, E. R.; Lee, Y. J.; Clemmer, D. E. Structural Transitions of Electrosprayed Ubiquitin Ions Stored in an Ion Trap over ~10 Ms to 30 s. *J. Phys. Chem. A* **2002**, *106* (42), 9976–9982.
(28) Badman, E. R.; Hoaglund-Hyzer, C. S.; Clemmer, D. E. Monitoring Structural Changes of Proteins in an Ion Trap over ~10−200 Ms: Unfolding Transitions in Cytochrome *c* Ions. *Anal. Chem.* **2001**, *73* (24), 6000–6007.
(29) Allen, S. J.; Eaton, R. M.; Bush, M. F. Structural Dynamics of Native-Like Ions in the Gas Phase: Results from Tandem Ion Mobility of Cytochrome *c*. *Anal. Chem.* **2017**, *89* (14), 7527–7534.
(30) Jurneczko, E.; Barran, P. E. How Useful Is Ion Mobility Mass Spectrometry for Structural Biology? The Relationship between Protein Crystal Structures and Their Collision Cross Sections in the Gas Phase. *The Analyst* **2011**, *136* (1), 20–28.
(31) Ruotolo, B. T.; Giles, K.; Campuzano, I.; Sandercock, A. M.; Bateman, R. H.; Robinson, C. V. Evidence for Macromolecular Protein Rings in the Absence of Bulk Water. *Science* **2005**, *310* (5754), 1658–1661.
(32) Breuker, K.; McLafferty, F. W. Native Electron Capture Dissociation for the Structural Characterization of Noncovalent Interactions in Native Cytochromec. *Angew. Chem. Int. Ed.* **2003**, *42* (40), 4900–4904.
(33) Breuker, K.; Oh, H.; Horn, D. M.; Cerda, B. A.; McLafferty, F. W. Detailed Unfolding and Folding of Gaseous Ubiquitin Ions Characterized by Electron Capture Dissociation. *J. Am. Chem. Soc.* **2002**, *124* (22), 6407–6420.
(34) Bleiholder, C.; Liu, F. C. Structure Relaxation Approximation (SRA) for Elucidation of Protein Structures from Ion Mobility Measurements. *J. Phys. Chem. B* **2019**, *123* (13), 2756–2769.
(35) Ruotolo, B. T.; Benesch, J. L. P.; Sandercock, A. M.; Hyung, S.-J.; Robinson, C. V. Ion Mobility–Mass Spectrometry Analysis of Large Protein Complexes. *Nat. Protoc.* **2008**, *3* (7), 1139–1152.
(36) Steinberg, M. Z.; Breuker, K.; Elber, R.; Gerber, R. B. The Dynamics of Water Evaporation from Partially Solvated Cytochrome c in the Gas Phase. *Phys. Chem. Chem. Phys.* **2007**, *9* (33), 4690.
(37) Warnke, S.; Von Helden, G.; Pagel, K. Protein Structure in the Gas Phase: The Influence of Side-Chain Microsolvation. *J. Am. Chem. Soc.* **2013**, *135* (4), 1177–1180.
(38) Zhou, W. Gas-Phase Ion-Electron and Ion-Photon Reactions for Structural Characterization of Protein Glycosylation. 211.
(39) Abramsson, M. L.; Sahin, C.; Hopper, J. T. S.; Branca, R. M. M.; Danielsson, J.; Xu, M.; Chandler, S. A.; Österlund, N.; Ilag, L. L.; Leppert, A.; Costeira-Paulo, J.; Lang, L.; Teilum, K.; Laganowsky, A.; Benesch, J. L. P.; Oliveberg, M.; Robinson, C. V.; Marklund, E. G.; Allison, T. M.; Winther, J. R.; Landreh, M. Charge Engineering Reveals the Roles of Ionizable Side Chains in Electrospray Ionization Mass Spectrometry. *JACS Au* **2021**, *1* (12), 2385–2393.
(40) Bryngelson, J. D.; Onuchic, J. N.; Socci, N. D.; Wolynes, P. G. Funnels, Pathways, and the Energy Landscape of Protein Folding: A Synthesis. *Proteins Struct. Funct. Genet.* **1995**, *21* (3), 167–195.
(41) Frauenfelder, H.; Sligar, S. G.; Wolynes, P. G. The Energy Landscapes and Motions of Proteins. *Science* **1991**, *254* (5038), 1598–1603.

(42) Matouschek, A.; Kellis, J. T.; Serrano, L.; Fersht, A. R. Mapping the Transition State and Pathway of Protein Folding by Protein Engineering. *Nature* **1989**, *340* (6229), 122–126.
(43) Jackson, S. E.; elMasry, N.; Fersht, A. R. Structure of the Hydrophobic Core in the Transition State for Folding of Chymotrypsin Inhibitor 2: A Critical Test of the Protein Engineering Method of Analysis. *Biochemistry* **1993**, *32* (42), 11270–11278.
(44) Fersht, A. R.; Sato, S. -Value Analysis and the Nature of Protein-Folding Transition States. *Proc. Natl. Acad. Sci.* **2004**, *101* (21), 7976–7981.
(45) Sosnick, T. R.; Dothager, R. S.; Krantz, B. A. Differences in the Folding Transition State of Ubiquitin Indicated by φ and ψ Analyses. *Proc. Natl. Acad. Sci.* **2004**, *101* (50), 17377–17382.
(46) Sabelko, J.; Ervin, J.; Gruebele, M. Observation of Strange Kinetics in Protein Folding. *Proc. Natl. Acad. Sci.* **1999**, *96* (11), 6031–6036.
(47) Rasmussen, B. F.; Stock, A. M.; Ringe, D.; Petsko, G. A. Crystalline Ribonuclease A Loses Function below the Dynamical Transition at 220 K. *Nature* **1992**, *357* (6377), 423–424.
(48) Vitkup, D.; Ringe, D.; Petsko, G. A.; Karplus, M. Solvent Mobility and the Protein 'Glass' Transition. *Nat. Struct. Biol.* **2000**, *7* (1).
(49) Zercher, B. P.; Hong, S.; Roush, A. E.; Feng, Y.; Bush, M. F. Are the Gas-Phase Structures of Molecular Elephants Enduring or Ephemeral? Results from Time-Dependent, Tandem Ion Mobility. *Anal. Chem.* **2023**, *95* (25), 9589–9597.
(50) Liu, F. C.; Ridgeway, M. E.; Park, M. A.; Bleiholder, C. Tandem Trapped Ion Mobility Spectrometry. *The Analyst* **2018**, *143* (10), 2249–2258.
(51) Went, H. M.; Benitez-Cardoza, C. G.; Jackson, S. E. Is an Intermediate State Populated on the Folding Pathway of Ubiquitin? *FEBS Lett.* **2004**, *567* (2–3), 333–338.
(52) Piana, S.; Lindorff-Larsen, K.; Shaw, D. E. Atomic-Level Description of Ubiquitin Folding. *Proc. Natl. Acad. Sci.* **2013**, *110* (15), 5915–5920.
(53) Went, H. M.; Jackson, S. E. Ubiquitin Folds through a Highly Polarized Transition State. *Protein Eng. Des. Sel.* **2005**, *18* (5), 229–237.
(54) Vijay-Kumar, S.; Bugg, C. E.; Wilkinson, K. D.; Cook, W. J. Three-Dimensional Structure of Ubiquitin at 2.8 A Resolution. *Proc. Natl. Acad. Sci.* **1985**, *82* (11), 3582–3585.
(55) Lange, O. F.; Lakomek, N.-A.; Farès, C.; Schröder, G. F.; Walter, K. F. A.; Becker, S.; Meiler, J.; Grubmüller, H.; Griesinger, C.; de Groot, B. L. Recognition Dynamics Up to Microseconds Revealed from an RDC-Derived Ubiquitin Ensemble in Solution. *Science* **2008**, *320* (5882), 1471–1475.
(56) Crespo, M. D.; Simpson, E. R.; Searle, M. S. Population of On-Pathway Intermediates in the Folding of Ubiquitin. *J. Mol. Biol.* **2006**, *360* (5), 1053–1066.
(57) Jourdan, M.; Searle, M. S. Insights into the Stability of Native and Partially Folded States of Ubiquitin: Effects of Cosolvents and Denaturants on the Thermodynamics of Protein Folding. *Biochemistry* **2001**, *40* (34), 10317–10325.
(58) Vallée-Bélisle, A.; Michnick, S. W. Multiple Tryptophan Probes Reveal That Ubiquitin Folds via a Late Misfolded Intermediate. *J. Mol. Biol.* **2007**, *374* (3), 791–805.
(59) Chung, H. S.; Ganim, Z.; Jones, K. C.; Tokmakoff, A. Transient 2D IR Spectroscopy of Ubiquitin Unfolding Dynamics. *Proc. Natl. Acad. Sci.* **2007**, *104* (36), 14237–14242.
(60) Kony, D. B.; Hünenberger, P. H.; van Gunsteren, W. F. Molecular Dynamics Simulations of the Native and Partially Folded States of Ubiquitin: Influence of Methanol Cosolvent, pH, and Temperature on the Protein Structure and Dynamics. *Protein Sci.* **2007**, *16* (6), 1101–1118.

(61) Brutscher, B.; Brüschweiler, R.; Ernst, R. R. Backbone Dynamics and Structural Characterization of the Partially Folded A State of Ubiquitin by ^{1}H, ^{13}C, and ^{15}N Nuclear Magnetic Resonance Spectroscopy. *Biochemistry* **1997**, *36* (42), 13043–13053.
(62) Michelmann, K.; Silveira, J. A.; Ridgeway, M. E.; Park, M. A. Fundamentals of Trapped Ion Mobility Spectrometry. *J. Am. Soc. Mass Spectrom.* **2015**, *26* (1), 14–24.
(63) Silveira, J. A.; Michelmann, K.; Ridgeway, M. E.; Park, M. A. Fundamentals of Trapped Ion Mobility Spectrometry Part II: Fluid Dynamics. *J. Am. Soc. Mass Spectrom.* **2016**, *27* (4), 585–595.
(64) Fernandez-Lima, F. A.; Kaplan, D. A.; Park, M. A. Note: Integration of Trapped Ion Mobility Spectrometry with Mass Spectrometry. *Rev. Sci. Instrum.* **2011**, *82* (12), 126106.
(65) Liu, F. C.; Kirk, S. R.; Bleiholder, C. On the Structural Denaturation of Biological Analytes in Trapped Ion Mobility Spectrometry – Mass Spectrometry. *The Analyst* **2016**, *141* (12), 3722–3730.
(66) Bleiholder, C.; Liu, F. C.; Chai, M. Comment on Effective Temperature and Structural Rearrangement in Trapped Ion Mobility Spectrometry. *Anal. Chem.* **2020**, *92* (24), 16329–16333.
(67) Chai, M.; Bleiholder, C. Structure-Elucidation of Human CCL5 by Integrating Trapped Ion Mobility Spectrometry-Mass Spectrometry (TIMS-MS) with Structure Relaxation Approximation (SRA) Analysis. *Int. J. Mass Spectrom.* **2021**, *469*, 116682.
(68) Liu, F. C.; Cropley, T. C.; Ridgeway, M. E.; Park, M. A.; Bleiholder, C. Structural Analysis of the Glycoprotein Complex Avidin by Tandem-Trapped Ion Mobility Spectrometry–Mass Spectrometry (Tandem-TIMS/MS). *Anal. Chem.* **2020**, *92* (6), 4459–4467.
(69) Cropley, T. C.; Liu, F. C.; Pedrete, T.; Hossain, M. A.; Agar, J. N.; Bleiholder, C. Structure Relaxation Approximation (SRA) for Elucidation of Protein Structures from Ion Mobility Measurements (II). Protein Complexes. *J. Phys. Chem. B* **2023**, *127* (25), 5553–5565.
(70) Jeanne Dit Fouque, K.; Garabedian, A.; Leng, F.; Tse-Dinh, Y.-C.; Ridgeway, M. E.; Park, M. A.; Fernandez-Lima, F. Trapped Ion Mobility Spectrometry of Native Macromolecular Assemblies. *Anal. Chem.* **2021**, *93* (5), 2933–2941.
(71) Molano-Arevalo, J. C.; Jeanne Dit Fouque, K.; Pham, K.; Miksovska, J.; Ridgeway, M. E.; Park, M. A.; Fernandez-Lima, F. Characterization of Intramolecular Interactions of Cytochrome *c* Using Hydrogen–Deuterium Exchange-Trapped Ion Mobility Spectrometry–Mass Spectrometry and Molecular Dynamics. *Anal. Chem.* **2017**, *89* (17), 8757–8765.
(72) Kirk, S. R.; Liu, F. C.; Cropley, T. C.; Carlock, H. R.; Bleiholder, C. On the Preservation of Non-Covalent Peptide Assemblies in a Tandem-Trapped Ion Mobility Spectrometer-Mass Spectrometer (TIMS-TIMS-MS). *J. Am. Soc. Mass Spectrom.* **2019**, *30* (7), 1204–1212.
(73) Liu, F. C.; Cropley, T. C.; Bleiholder, C. Elucidating Structures of Protein Complexes by Collision-Induced Dissociation at Elevated Gas Pressures. *J. Am. Soc. Mass Spectrom.* **2023**, *34* (10), 2247–2258.
(74) Liu, F. C.; Kirk, S. R.; Caldwell, K. A.; Pedrete, T.; Meier, F.; Bleiholder, C. Tandem Trapped Ion Mobility Spectrometry/Mass Spectrometry (tTIMS/MS) Reveals Sequence-Specific Determinants of Top-Down Protein Fragment Ion Cross Sections. *Anal. Chem.* **2022**, *94* (23), 8146–8155.
(75) Hernandez, D. R.; DeBord, J. D.; Ridgeway, M. E.; Kaplan, D. A.; Park, M. A.; Fernandez-Lima, F. Ion Dynamics in a Trapped Ion Mobility Spectrometer. *The Analyst* **2014**, *139* (8), 1913–1921.

(76) Chai, M.; Young, M. N.; Liu, F. C.; Bleiholder, C. A Transferable, Sample-Independent Calibration Procedure for Trapped Ion Mobility Spectrometry (TIMS). *Anal. Chem.* **2018**, *90* (15), 9040–9047.
(77) Silveira, J. A.; Ridgeway, M. E.; Park, M. A. High Resolution Trapped Ion Mobility Spectrometery of Peptides. *Anal. Chem.* **2014**, *86* (12), 5624–5627.
(78) Stow, S. M.; Causon, T. J.; Zheng, X.; Kurulugama, R. T.; Mairinger, T.; May, J. C.; Rennie, E. E.; Baker, E. S.; Smith, R. D.; McLean, J. A.; Hann, S.; Fjeldsted, J. C. An Interlaboratory Evaluation of Drift Tube Ion Mobility–Mass Spectrometry Collision Cross Section Measurements. *Anal. Chem.* **2017**, *89* (17), 9048–9055.
(79) Lee, J.; Chai, M.; Bleiholder, C. Differentiation of Isomeric, Nonseparable Carbohydrates Using Tandem-Trapped Ion Mobility Spectrometry–Mass Spectrometry. *Anal. Chem.* **2022**, *95*, 747−757.
(80) Berendsen, H. J. C.; van der Spoel, D.; van Drunen, R. GROMACS: A Message-Passing Parallel Molecular Dynamics Implementation. *Comput. Phys. Commun.* **1995**, *91* (1–3), 43–56.
(81) Jorgensen, W. L.; Tirado-Rives, J. The OPLS Potential Functions for Proteins. Energy Minimizations for Crystals of Cyclic Peptides and Crambin. *J. Am. Chem. Soc.* **1988**, *110*, 1657–1666.
(82) Kaminski, G. A.; Friesner, R. A.; Tirado-Rives, J.; Jorgensen, W. L. Evaluation and Reparametrization of the OPLS-AA Force Field for Proteins via Comparison with Accurate Quantum Chemical Calculations on Peptides. *J. Phys. Chem. B* **2001**, *105* (28), 6474–6487.
(83) Bleiholder, C.; Wyttenbach, T.; Bowers, M. T. A Novel Projection Approximation Algorithm for the Fast and Accurate Computation of Molecular Collision Cross Sections (I). Method. *Int. J. Mass Spectrom.* **2011**, *308* (1), 1–10.
(84) Bleiholder, C.; Contreras, S.; Bowers, M. T. A Novel Projection Approximation Algorithm for the Fast and Accurate Computation of Molecular Collision Cross Sections (IV). Application to Polypeptides. *Int. J. Mass Spectrom.* **2013**, *354–355*, 275–280.
(85) Bleiholder, C.; Contreras, S.; Do, T. D.; Bowers, M. T. A Novel Projection Approximation Algorithm for the Fast and Accurate Computation of Molecular Collision Cross Sections (II). Model Parameterization and Definition of Empirical Shape Factors for Proteins. *Int. J. Mass Spectrom.* **2013**, *345–347*, 89–96.
(86) Anderson, S. E.; Bleiholder, C.; Brocker, E. R.; Stang, P. J.; Bowers, M. T. A Novel Projection Approximation Algorithm for the Fast and Accurate Computation of Molecular Collision Cross Sections (III): Application to Supramolecular Coordination-Driven Assemblies with Complex Shapes. *Int. J. Mass Spectrom.* **2012**, *330–332*, 78–84.
(87) Bleiholder, C.; Johnson, N. R.; Contreras, S.; Wyttenbach, T.; Bowers, M. T. Molecular Structures and Ion Mobility Cross Sections: Analysis of the Effects of He and N_2 Buffer Gas. *Anal. Chem.* **2015**, *87* (14), 7196–7203.
(88) France, A. P.; Migas, L. G.; Sinclair, E.; Bellina, B.; Barran, P. E. Using Collision Cross Section Distributions to Assess the Distribution of Collision Cross Section Values. *Anal. Chem.* **2020**, *92*, 4340−4348.
(89) Fenwick, R. B.; Esteban-Martín, S.; Richter, B.; Lee, D.; Walter, K. F. A.; Milovanovic, D.; Becker, S.; Lakomek, N. A.; Griesinger, C.; Salvatella, X. Weak Long-Range Correlated Motions in a Surface Patch of Ubiquitin Involved in Molecular Recognition. *J. Am. Chem. Soc.* **2011**, *133* (27), 10336–10339.

(90) Phillips, J. C. Stretched Exponential Relaxation in Molecular and Electronic Glasses. *Rep. Prog. Phys.* **1996**, *59* (9), 1133–1207.
(91) Mauro, J. C.; Smedskjaer, M. M. Statistical Mechanics of Glass. *J. Non-Cryst. Solids* **2014**, *396–397*, 41–53.
(92) Ediger, M. D.; Angell, C. A.; Nagel, S. R. Supercooled Liquids and Glasses. *J Phys Chem* **1996**, *100*, 13200–13212.